JACS
JOURNAL OF THE AMERICAN CHEMICAL SOCIETY

ARTICLE

pubs.acs.org/JACS

Thiocyanate-Capped Nanocrystal Colloids: Vibrational Reporter of Surface Chemistry and Solution-Based Route to Enhanced Coupling in Nanocrystal Solids

Aaron T. Fafarman,[†] Weon-kyu Koh,[‡] Benjamin T. Diroll,[‡] David K. Kim,[§] Dong-Kyun Ko,[§] Soong Ju Oh,[§] Xingchen Ye,[‡] Vicky Doan-Nguyen,[§] Michael R. Crump,[§] Danielle C. Reifsnyder,[‡] Christopher B. Murray,[‡,§] and Cherie R. Kagan*[,†,‡,§]

[†]Department of Electrical and Systems Engineering, [‡]Department of Chemistry, and [§]Department of Materials Science and Engineering, University of Pennsylvania, Philadelphia, Pennsylvania 19104, United States

Supporting Information

ABSTRACT: Ammonium thiocyanate (NH_4SCN) is introduced to exchange the long, insulating ligands used in colloidal nanocrystal (NC) synthesis. The short, air-stable, environmentally benign thiocyanate ligand electrostatically stabilizes a variety of semiconductor and metallic NCs in polar solvents, allowing solution-based deposition of NCs into thin-film NC solids. NH_4SCN is also effective in replacing ligands on NCs after their assembly into the solid state. The spectroscopic properties of this ligand provide unprecedented insight into the chemical and electronic nature of the surface of the NCs. Spectra indicate that the thiocyanate binds to metal sites on the NC surface and is sensitive to atom type and NC surface charge. The short, thiocyanate ligand gives rise to significantly enhanced electronic coupling between NCs as evidenced by large bathochromic shifts in the absorption spectra of CdSe and CdTe NC thin films and by conductivities as high as $(2 \pm 0.7) \times 10^3\ \Omega^{-1}\ cm^{-1}$ for Au NC thin films deposited from solution. NH_4SCN treatment of PbTe NC films increases the conductivity by 10^{13}, allowing the first Hall measurements of nonsintered NC solids, with Hall effect mobilities of $2.8 \pm 0.7\ cm^2/(V \cdot s)$. Thiocyanate-capped CdSe NC thin films form photodetectors exhibiting sensitive photoconductivity of $10^{-5}\ \Omega^{-1}\ cm^{-1}$ under 30 mW/cm^2 of 488 nm illumination with $I_{photo}/I_{dark} > 10^3$ and form *n*-channel thin-film transistors with electron mobilities of $1.5 \pm 0.7\ cm^2/(V \cdot s)$, a current modulation of $>10^6$, and a subthreshold swing of 0.73 V/decade.

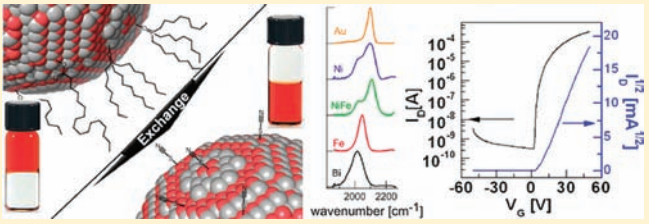

INTRODUCTION

Colloidal nanocrystals (NCs) are of tremendous scientific and technological interest for their size- and shape-tunable optical, electrical, and magnetic properties[1−5] as well as their propensity to self-assemble from solution into nanostructured solids.[5−10] This has spurred research into their use as low-cost, solution-processable, and printable NC conductors,[11] thin-film-based optoelectronic devices, such as photovoltaics,[12−14] photodetectors,[14,15] and light-emitting diodes,[16,17] and the active material in electronic,[18−21] thermoelectric,[22−24] and magnetic[25] recording applications. State-of-the-art wet-chemical techniques for synthesizing colloidal NCs with a high degree of size, shape, and phase homogeneity rely upon capping the NC surface with organic surfactants to control NC growth and to stabilize NC dispersions in solution. However, when colloidal NCs are assembled into NC solids, these long, bulky, insulating ligands prevent the close approach of NCs and the strong interparticle coupling desirable for device applications.

Two strategies for the postsynthetic replacement of the original, long, bulky ligands with shorter, compact ligands have been used to enhance interparticle coupling in solution-processed, NC-based thin films. (1) Solid exchange involves first assembling the NCs into a solid and then treating the resulting film with a solution containing the new ligand.[26−30] This has been shown to effectively displace the original, bulky ligands, leaving the shorter, compact ligands behind, but leads to cracking and void spaces due to the lost volume and therefore requires subsequent steps to backfill defects with additional NCs. (2) Solution exchange entails replacing the original organic surfactants with smaller ligands capable of preserving the solution dispersibility of the NCs. Solution exchange is particularly attractive as it enables the formation of dense solids with short interparticle separation directly, with no discernible shrinkage or cracking, via a single processing step amenable to large-scale industrial thin-film production techniques, e.g., spin-casting, spraying, or roll-to-roll printing. Only a handful of ligands have been developed for NC solution exchange, and there are limitations to each: pyridine leads to relatively modest increases in electronic coupling,[28,31] the molecular metal chalcogenide system demonstrates impressive electronic coupling[32,33] but involves toxic materials incompatible with many device fabrication modalities, and nitrosonium tetrafluoroborate is limited to acid-stable materials.[34] During the preparation of this paper, a new

Received: July 7, 2011
Published: August 17, 2011

Scheme 1. Ligand Exchange

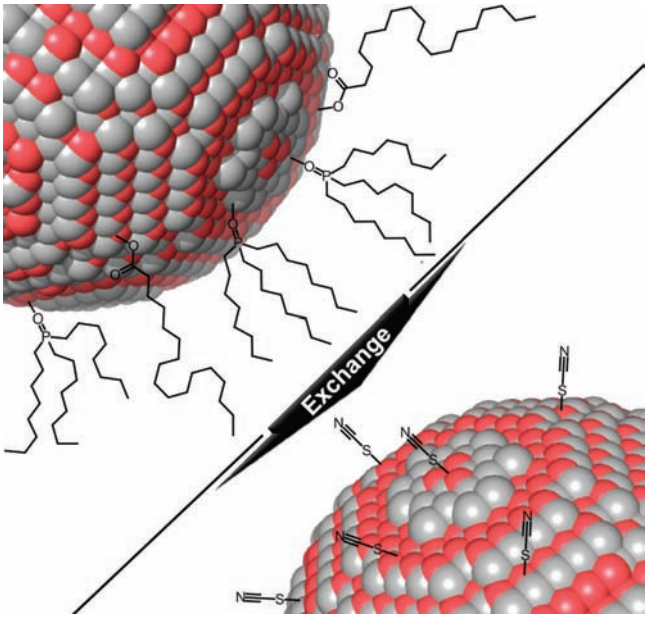

ligand-replacement strategy using chalcogenide anions was reported by Talapin et al., demonstrating the active interest in the community to develop alternatives.[35]

We introduce ammonium thiocyanate (NH_4SCN) as a new, short, inorganic ligand, capable of promoting solution dispersibility for a wide range of semiconductor and metal NCs as well as serving as a useful agent for solid-state exchange. NH_4SCN is produced worldwide on the kiloton scale and is air-stable and environmentally benign. The distinct vibrational spectrum, high oscillator strength, simple linear structure, and demonstrated environmental spectral sensitivity[36] make thiocyanate (SCN) an ideal reporter with which to probe the chemistry and local environment at the surface of NCs in solution and in the solid state. In prior studies, SCN has been shown to adsorb to large (>20 nm) metal nanoparticles in aqueous dispersions, where significant surface-enhanced Raman scattering of the CN stretch is observed,[37,38] and has been hypothesized to exist as an intermediate in the thermolysis of 1-substituted 5-thiotetrazole-based NC ligands.[39] We show by infrared absorption spectroscopy of the CN stretch that SCN binds metal sites on the surface of a variety of metallic and semiconducting NCs and provides a measure of the net charge at the NC surface. SCN is also used to follow changes at the NC surface during assembly of NC solids or exchange of the ligands in the solid state. As depicted in Scheme 1, the thiocyanate ligand represents a substantial decrease in ligand size, making possible the short interparticle separations necessary for strong electronic communication between NCs. This is demonstrated by measured bathochromic shifts in NC absorption and enhanced conductivities and carrier mobilities in NC solids. We harness the strong electronic coupling between NCs to demonstrate high-performance thin-film photodetectors and field-effect transistors from NC thin films deposited using this ligand chemistry.

EXPERIMENTAL SECTION

Materials. A list of chemicals used and the commercial source for each is given in the Supporting Information.

NC Synthesis. *CdS NCs.* Cadmium sulfide NCs were made using a modification of a literature synthesis:[40] In a typical reaction, a 125 mL three-neck flask was loaded with 350 mg of CdO, 66.5 mL of octadecene, and 3.5 mL of oleic acid and heated to 120 °C, held under vacuum for 30 min, and then heated to 300 °C until clear. The flask was then cooled to 120 °C and held under vacuum for 1 h. A 2.8 mL volume of 0.5 M sulfur solution dissolved in octadecene was injected into the flask, which was then heated under nitrogen to 220 °C and held for 1 h. A UV−vis spectrum of a typical NC sample is available in the Supporting Information (Figure S1).

CdSe NCs. Cadmium selenide NCs were synthesized using a modified literature procedure:[41] In a typical reaction, 20.0 g of trioctylphosphine oxide, 20.0 g of octadecylamine, and 2.1 g of cadmium stearate were dried under vacuum at 120 °C for 1 h and then heated to 320 °C under nitrogen, whereupon 10.0 mL of 1.25 M selenium in tributylphosphine solution was rapidly injected. Growth was continued at 290 °C.

ZnSe NCs. Zinc selenide NCs in hexanes were synthesized using a modified literature procedure[42] by replacing tetracosane with a 1:1 solution of squalane and octadecene. The UV−vis spectrum of a typical NC sample is available in the Supporting Information (Figure S1).

Ni NCs. Ni NCs were synthesized using a modified literature procedure:[43] A 1 mmol portion of $Ni(acac)_2$, 30 mmol of oleylamine, and 30 mmol of trioctylphosphine (97%) in 15 mL of benzyl ether were evacuated in a three-neck flask at 100 °C for 30 min. The temperature was increased to 230 °C and maintained for 15 min.

NiFe NCs. The intermetallic NiFe NCs were synthesized starting with 1 mmol of $Ni(acac)_2$ and 1 mmol of $Fe(CO)_5$. $Ni(acac)_2$, 2 mmol of oleic acid, and 1 mmol of tributylphosphine in 20 mL of benzyl ether were heated to 200 °C, at which point $Fe(CO)_5$ was injected. The solution was maintained at 220 °C for 30 min.

CdTe, PbS, PbSe, PbTe, Au, Fe, and Bi NCs. CdTe,[44] PbS,[45] PbSe,[46] PbTe,[47] Au,[48] Fe,[49] and Bi[50] NCs were synthesized according to previously reported methods. With the exception of Au and ZnSe NCs, all purification was carried out in a nitrogen atmosphere, using anhydrous solvents.

Solid Exchange. As-synthesized NCs were dispersed in hexanes and assembled into thin films (drop-cast) on sapphire, glass, or polished silicon substrates. Self-assembled monolayers of (3-mercaptopropyl)-trimethoxysilane (MPTS) were necessary on the glass and silicon substrates to prevent the delamination of NC films after exchange and were prepared according to literature procedures.[51] For comparisons of organic ligand coverage before and after exchange, the films were immersed in 2-propanol solution for 10 min to remove any nonspecifically bound ligands. Ligand exchange was performed by immersing the films in 130 mM (1%, w/v) NH_4SCN in acetone for 1 min, followed by immersion in two successive baths of pure acetone for 1 min each.

Solution Exchange. In a typical procedure 0.5 mL of 130 mM NH_4SCN in acetone was added to 1 mL of a dispersion of as-synthesized NCs in hexanes and the resulting solution agitated for 1 min. Complete flocculation was observed within seconds. The slurry was centrifuged at 2000*g* for 1 min and the supernatant discarded. A 1 mL volume of acetone was added, the slurry agitated for 1 min and centrifuged at 2000*g* for 1 min, and the supernatant discarded. A 1 mL volume of DMSO was added to the pellet, and the mixture was gently agitated until the NCs were fully dispersed. After centrifugation of the resultant dispersion at 3000*g* for 4 min, no solid was observed for the solution-dispersible materials reported. Dispersions were stable for days to months.

For CdSe NCs used in the photoconductivity and field-effect transistor measurements, a more exhaustive exchange procedure was followed and all steps were performed in a nitrogen atmosphere with anhydrous solvents. A 0.5 mL volume of 130 mM NH_4SCN in acetone was added to 1 mL of a dispersion of CdSe NCs in hexanes (the concentration was controlled by adjusting the optical density of the dispersion at the peak of the lowest energy excitonic absorption feature,

e.g., 583 nm for 3.9 nm diameter NCs,[52] to a value of 10−20 per centimeter) and the resulting solution stirred with a vortexing mixer at 3000 rpm for 2 min. Complete flocculation was observed within seconds. The slurry was centrifuged at 2000*g* for 1 min and the supernatant discarded. A 1 mL volume of tetrahydrofuran was added, the slurry stirred at 3000 rpm for 2 min and centrifuged at 2000*g* for 1 min, and the supernatant discarded. A 1 mL volume of toluene was added, the slurry stirred at 3000 rpm for 1 min and centrifuged at 2000*g* for 1 min, and the supernatant discarded. A 0.2 mL volume of dimethylformamide (DMF) was added to the pellet, and the mixture was gently agitated until the NCs were fully dispersed. In contrast to the more stable dispersions formed by the typical procedure, these dispersions slowly become turbid over the course of 1 h and must be used within minutes of preparation.

Dynamic Light Scattering. CdSe and ZnSe samples were exchanged according to the typical solution exchange procedure described above. ζ potential measurements were performed on a Delsa Nano C (Beckman Coulter) instrument using a quartz cell. Dynamic light scattering (DLS) measurements were carried out on a Zetasizer NanoS (Malvern). All ζ potential measurements were taken from six measurements of 140 scans at 60 V bias; DLS data are reported averages of at least 10 measurements of 15 scans.

Infrared Absorption Spectroscopy. All spectra were taken in transmission mode on a model 6700 Fourier transform infrared (FT-IR) spectrometer (formerly Nicolet, now Thermo-Fisher) at a spectral resolution of 4 cm^{-1}. Potassium bromide and either trioctylphosphine (90%) or recrystallized NH_4SCN were combined and pressed into pellets with a hand press. Spectra of NC films were taken on MPTS-treated, double-side-polished silicon substrates. CdSe NC films were also taken on sapphire substrates to allow transmission from the mid-IR through the UV−vis regions of the spectrum for subsequent visible absorption studies. For these combined IR/UV−vis measurements of CdSe NC films, thicker films were required, which were made by 10 successive rounds of drop-casting and solid exchange; all other experiments were measured from a single deposition. Data shown are the composite of three spectra of independently prepared films, averaged together. Spectra of CdSe and ZnSe NC dispersions in dimethyl sulfoxide (DMSO) were taken in a demountable liquid cell with sapphire windows and 50 μm Teflon spacers (Harrick). Dispersions were prepared according to the typical solution exchange procedure described above. For the comparison between typical and more rigorous removal of excess NH_4SCN, an additional acetone washing step was employed before dispersion of the NCs in DMSO. For isotopic studies, the NCs were first exchanged with NH_4SCN, as described in the typical solution exchange procedure, and centrifuged, and the supernatant was discarded. Then 0.5 mL of 100 mM (1%, w/v) ^{15}N-labeled potassium thiocyanate ($KSC^{15}N$) in acetone was added, the slurry agitated for 1 min and centrifuged at 2000*g* for 1 min, and the supernatant discarded. This step was repeated one additional time to ensure removal of the non-^{15}N-labeled thiocyanate. The NCs were then washed with acetone either once or, for the comparison to more rigorous NH_4SCN removal, twice and then dispersed in DMSO.

UV−Vis Absorption Spectroscopy. Spectra were taken in transmission mode on a Cary 5000 spectrophotometer (formerly Varian Inc., now Agilent Technologies) at 2 nm spectral bandwidth. All sample preparation steps were performed in a nitrogen atmosphere. The excitonic absorption spectra were measured for the same CdSe NC films on sapphire and CdSe NC dispersions in the sapphire liquid cell as those described for the IR experiments. The optical density of the lowest energy excitonic absorption feature at 583 nm was used to scale the IR spectra. CdSe NCs after solution exchange were deposited either by drop-casting from DMF onto glass slides or a quartz substrate held at 50 °C or by spin-casting onto sapphire substrates. NC films were annealed by placing samples on a hot plate with the surface temperature held at 150 or 250 °C for 10 min and then allowing the samples to return to room temperature. Absorption spectra were taken in air immediately after removal of the samples from a nitrogen atmosphere.

Electron Microscopy. High-resolution scanning electron micsroscopy (SEM) was performed on a model 7500F microscope (JEOL) operating at 15.0 kV.

Conductivity Measurements. Gold electrodes (20 nm) were deposited on top of a UV-ozone-treated (30 min) polyimide film (Dupont) by thermal evaporation through a shadow mask. Channel lengths (L) and widths (W) ranged from 30 to 200 μm with a constant W/L of 15 for all devices. Au NC samples, size-tunable from 5 to 8 nm in diameter, were exchanged using the typical solution exchange procedure, with the modifications that only 0.1 mL of 130 mM NH_4SCN was used for 1 mL of oleylamine-capped Au NCs dispersed in hexanes (the Au NC concentration was determined using the optical density of the dispersion at 520 nm and was in the range of 80−150 for a 1 cm path length), and the washed pellet was dispersed in 50 μL of DMSO. A 20 μL volume of this solution was deposited on the patterned polyimide substrate and evaporated to dryness at 60 °C at a reduced pressure of 400 Torr. Wide-angle X-ray scattering data for identically prepared films on silicon substrates exhibit no evidence for sintering (Supporting Information, Figure S2). Contact to the electrodes was made using a model PM5 probe station (Karl Suss) connected to a model 2400 multimeter (Kiethley). Conductivity showed no dependence on the channel length, as expected for a fixed W/L ratio. Values reported were calculated from seven independent electrode pairs from multiple substrates, assuming the conductive channel to have dimensions equal to the channel's cross-section.

Hall Effect Measurement. All measurements and sample preparation steps were conducted under a nitrogen atmosphere. PbTe NCs (7.5 nm) were drop-cast on MPTS-treated cover glass and the films treated using the solid exchange procedure described above. Five successive rounds of deposition were required to make thick, densely packed films (see the Supporting Information, Figure S3). After selectively cleaning the perimeter of a drop-cast film with a wooden tip, four electrical contacts were made at each corner in the van der Pauw geometry using silver paste (Leitsilber 200, Ted Pella). Four-point probe resistivity and Hall effect measurements were performed using an MMR Technologies H-50 measurement system with a 0.5 T magnet. The film thickness was measured using a profilometer (Alpha Step 200, Tencor Instruments). All the measurements were conducted in an inert glovebox atmosphere following solid exchange.

Photoconductivity and Spectral Response. Precleaned quartz was used as a substrate onto which 20 nm thick Au electrodes (10 μm channel length, 150 μm channel width) were photolithographically defined. Thin films of CdSe NCs were drop-cast from DMF, after the more exhaustive solution exchange procedure described above, onto the substrate held at 50 °C. The active area was sealed using epoxy (5 min, ITW Devcon) under a glass coverslip in a nitrogen atmosphere. Devices were illuminated with the 488 nm line of an Innova 70C spectrum Ar:Kr laser (Coherent). Neutral density filters were used to control the illumination intensity. Photocurrents and dark currents were recorded by a model 6517B electrometer (Keithley). The spectral response of an identically prepared sample was measured on a FluoroLog-3 fluorescence spectrometer (Jobin-Yvon). Light from the excitation monochromator, at 10 nm spectral bandwidth, was chopped at 140 Hz and the sample held at a 1 V bias using a model 2400 source measure unit (Keithley). The larger spectral bandwidth in the photoconductivity experiments was required for uniform sample illumination, but introduces broadening of the spectral features relative to the UV−vis absorption measurements. Wired in series with the sample was a model SR830 lock-in detector (Stanford Research Systems), locked into the 140 Hz chopper signal. The lock-in detector output was directed into a signal capture card built into the FluoroLog-3.

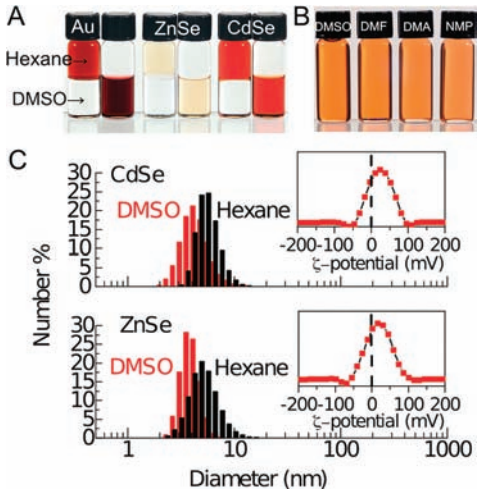

Figure 1. Solution dispersion of various NCs after exchange with NH_4SCN. (A) Biphasic mixtures of hexane and DMSO with as-synthesized NCs on the left of each pair and NCs treated with NH_4SCN, washed, and redispersed in DMSO with hexane added to the top on the right. From left to right: Au, ZnSe, and CdSe. (B) From left to right: CdSe-SCN dispersed in DMSO, DMF, DMA, and NMP. (C) Size distributions based on dynamic light scattering for ZnSe and CdSe before (black) and after (red) ligand exchange. The inset shows the ζ potential after exchange, measured by light scattering under applied bias.

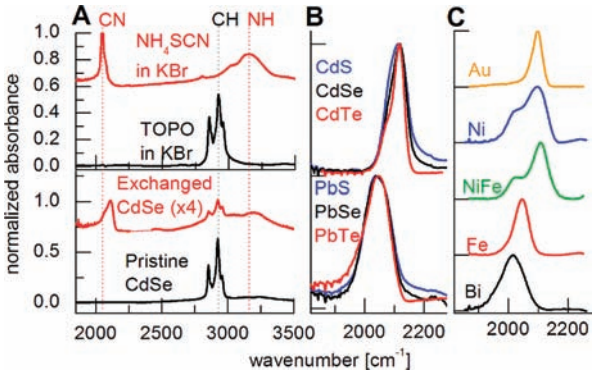

Figure 2. Transmission IR spectra in the solid state. (A) Mid-IR spectra of NH_4SCN (red) and technical grade TOPO (black) in a KBr pellet, compared to the IR spectrum of CdSe NCs deposited on sapphire substrates, either before (black) or after (red) exchange with NH_4SCN. Dashed red lines and a dashed black line indicate the CN and NH stretches of NH_4SCN and the CH region of TOPO, respectively. The CdSe films are scaled to the magnitude of the absorption maximum of the first excitonic feature at 586 nm, measured on the same samples, and the exchanged film is further scaled up by a factor of 4. Spectra are the composite of three independent sample preparations, averaged together. (B, C) Spectra in the CN stretching region of cadmium and lead chalcogenide NC films (B) and metal NC films (C) after exchange with NH_4SCN.

Field-Effect Transistor Fabrication and Characterization. All fabrication and characterization steps were performed under a nitrogen atmosphere. CdSe NCs were exchanged by the more exhaustive solution exchange procedure described above, dispersed in DMF to an optical density of 100 at the peak of lowest energy excitonic absorption, and used immediately after exchange. This dispersion was filtered through a 0.2 μm PTFE filter. CdSe NC films were deposited by spin-casting the dispersion at 500 rpm for 30 s, followed by 800 rpm for 30 s, to yield uniform continuous films on *n*-doped Si wafers with 130 nm thermally grown SiO_2, which served as the gate and gate dielectric of the field-effect transistors (FETs), respectively. Indium source and drain electrodes (40 nm) were deposited by thermal evaporation through a shadow mask to form top contact, bottom gate thin-film FETs. Channel lengths (L) and widths (W) ranged from 30 to 200 μm with a constant W/L of 15 for all devices. Devices were subsequently annealed at 250 °C for 10 min. Device characterization was performed on a model 4156C semiconductor parameter analyzer (Agilent) in combination with a Karl Suss PM5 probe station mounted in the nitrogen glovebox.

RESULTS AND DISCUSSION

Solution Exchange. Wet-chemically synthesized semiconductor or metallic NCs capped with long, insulating surfactants such as trioctylphospine oxide (TOPO) or oleic acid (OLA) were dispersed in a nonpolar solvent such as hexanes. Addition of NH_4SCN causes immediate flocculation of the NCs. Figure 1A shows that, in biphasic solutions of hexanes and DMSO, the NCs partition completely into the nonpolar phase prior to exchange and completely into the polar phase after exchange. Pictured here from left to right are Au, ZnSe, and CdSe NC dispersions. CdS NCs were also tested and shown to form stable dispersions. Figure 1B exhibits a range of polar solvents tested and found to redisperse CdSe NCs after exchange, in addition to DMSO: DMF, dimethyl amide (DMA), and *N*-methylpyrrolidone (NMP). DLS data shown in Figure 1C demonstrate that ZnSe and CdSe are monomerically dispersed both before and after exchange. The reduction in the average effective diameter after exchange is expected on the basis of the smaller hydrodynamic cross-section of the new ligands. In contrast, Au NCs are suspended in DMSO as small clusters of aggregated NCs with size distribution centered at 20 nm (Supporting Information, Figure S4). Exchange of ferromagnetic Ni NCs was also tested. The Ni NCs aggregated into clusters centered at a hydrodynamic radius of 200 nm in DMSO (Supporting Information, Figure S4). While the latter technically meets the accepted definition of a colloidal dispersion,[53] these aggregates are outside the size range of interest for this study and are not discussed in what follows. Further testing and optimization are currently under way to define conditions to form stable, monomeric dispersions from an even wider variety of NCs with this ligand. The insets of Figure 1C show ζ potential values for thiocyanate-treated CdSe and ZnSe NCs of 25 ± 3 and 20 ± 3 mV, respectively, suggesting that these NC dispersions are stabilized by electrostatic repulsion between particles, as found in other examples of colloidal NCs in polar solvents.[33−35]

Solid Exchange. Alternatively, the original, organic ligands (surfactants) used in NC synthesis can be removed after assembly of the NCs into a solid film, which expands the range of materials that can be treated by NH_4SCN. The exchange can be followed by comparing the vibrational spectrum before and after exchange. In Figure 2A, the distinct vibrational fingerprints of NH_4SCN near 2050 cm^{-1} (top, red curve) and hydrocarbons such as TOPO near 2900 cm^{-1} (top, black curve) are evident. For CdSe NCs before and after solid exchange (bottom, black and red curves, respectively), the areas of these peaks are used to quantify the removal of the original ligands and their replacement with thiocyanate. After both spectra were scaled to the optical density at the first excitonic resonance of the NCs, the relative integrated area of the CH stretching region after exchange (magnified 4-fold for visualization) indicates that >90% of the insulating organic surfactants have been removed.

dx.doi.org/10.1021/ja206303g |*J. Am. Chem. Soc.* 2011, 133, 15753–15761

The CN stretching region reveals details of the chemical nature of the SCN binding site on the NC surface. Figure 2B compares the CN vibrational fingerprints for cadmium chalcogenides CdS, CdSe, and CdTe consistently centered near 2120 cm^{-1}, with the lead analogues PbS, PbSe, and PbTe consistently centered near 2040 cm^{-1}. The identity of the metal, not the chalcogen, determines the thiocyanate vibrational frequency. The 80 cm^{-1} separation in frequency between these two sets of chalcogenide NCs is comparable to the approximately 60 cm^{-1} difference in the CN stretching frequency of model small molecules $Pb(NCS)_2$ and $Cd(SCN)_2$ (Supporting Information, Figure S5). This strongly suggests that the positively charged NC surface sites that bind the SCN are lead or cadmium atoms. In Figure 2C, the thiocyanate is shown to bind to metallic NCs, Au, Ni, and Fe and semimetallic Bi, where the CN mode exhibits a variation in stretching frequency extending over nearly 100 cm^{-1}. This chemical specificity is evidence that SCN is chemisorbed, not physisorbed, to the NC surface.

SCN is an ambidentate ligand; i.e., it is found in both S- and N-bound coordination modes.[54] The frequencies of the nitrile stretch suggest a predominant S-bound mode for the SCN (as depicted for CdSe in Scheme 1) when bound to gold or cadmium chalcogenide NCs. Both exhibit frequencies well within the range derived from small inorganic complexes associated with S-bound modes (2085−2130 cm^{-1}); however, due to the broad linewidths observed in the NC spectra, N-bound modes (2050−2100 cm^{-1}) cannot be excluded.[36] In contrast, in the series of lead chalcogenide NCs in Figure 2B, the nitrile stretch is found very near the value observed for N-bound SCN in $Pb(NCS)_2$ (see ref 55 and the Supporting Information, Figure S5). However, assignments of binding mode based on SCN vibrational frequency are occasionally inconclusive, particularly for thiocyanate complexes with lead, which are systematically lower in frequency than those of most metals.[55,56] More definitive measurement by NMR[56,57] is currently being pursued (see the Supporting Information, Figure S6).

Dynamic Properties of the Thiocyanate Ligand in Solution. Transmission IR spectra taken of colloidal solutions of NH_4SCN-treated ZnSe and CdSe (ZnSe-SCN and CdSe-SCN, respectively) NCs allow direct observation of the dynamic behavior of the ligand in solution. In the transmission IR spectrum shown at the top of Figure 3A of ZnSe NCs with SCN ligands in DMSO, scaled to unity at the absorption maximum, two overlapping peaks are evident: one at 2060 cm^{-1} and one at 2080 cm^{-1} (blue curve). To account for these two peaks, there are two obvious states available to the SCN^- anion that each maintain charge balance: (1) ionically bound to positive charge sites on the NC surface or (2) free in solution with charge balance maintained by the initial ammonium (NH_4^+) counterion. However, a third possibility is for SCN^- anions to be dissociated from, but charge-balanced by, a positive charge site on the NC surface (3). The spectrum of pure NH_4SCN in DMSO (dashed, black curve) shows that free SCN^- is found at 2060 cm^{-1}. Scenarios 2 and 3, both involving free SCN^-, are therefore also expected at 2060 cm^{-1}, and we turn to solubility differences to distinguish between them. Acetone is an antisolvent for ZnSe-SCN NCs but readily dissolves SCN^- salts; thus by washing the NCs with acetone, case 2, the free SCN^- charge balanced by NH_4^+, should be removed, leaving behind cases 1 and 3, the SCN^- bound and charge balanced by the NC surface, respectively. Performing an extra washing step with acetone leads to a small reduction in the integrated area of the

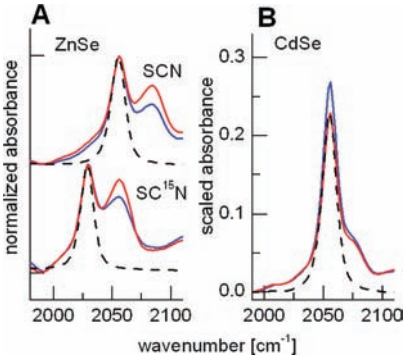

Figure 3. Transmission IR spectra of CdSe-SCN and ZnSe-SCN NCs in DMSO. (A) Normalized absorption spectra of ZnSe-SCN NCs in the CN stretching region. Top: treated with NH_4SCN and washed once (blue) or twice (red) with acetone prior to dispersion in DMSO. The black curve is for 100 mM NH_4SCN in DMSO. All spectra normalized to the peak at 2060 cm^{-1}. Bottom: treated first with NH_4SCN and then $KSC^{15}N$ and then washed once (blue) or twice (red) with acetone. The black curve is for 100 mM $KSC^{15}N$ in DMSO. All spectra normalized to the peak at 2030 cm^{-1}. (B) Spectra in the CN stretching region of CdSe-SCN NCs, scaled to the magnitude of the absorption maximum of the first excitonic feature at 583 nm, measured on the same samples. After exchange, CdSe-SCN NCs are washed either once (blue) or twice (red) with acetone and then redispersed in DMSO. The absorptivity (*y*-axis) is scaled to an NC concentration of 1 mM, defined using the published absorption coefficient for CdSe NCs. 100 mM NH_4SCN in DMSO, scaled down by a factor of 3, in black.

CN stretch relative to the UV−vis absorption of the sample. This is driven by a slightly diminished intensity of the 2060 cm^{-1} peak, which is seen in the red curve in the upper panel of Figure 3A as an increase in the ratio of the 2080 cm^{-1} peak to the 2060 cm^{-1} peak after renormalization of the latter to an absorbance of 1. The decrease in the 2060 cm^{-1} peak is assigned to removal of the small amount of excess SCN^- charge balanced by NH_4^+ (scenario 2). The minimum number of SCN^- anions required to charge balance the NC surface sites are left behind, with the peak at 2060 cm^{-1} assigned to those SCN^- free in solution (scenario 3) and the peak at 2080 cm^{-1} assigned to those SCN^- bound to the NC surface (scenario 1). Isotope labeling experiments provide evidence that this is a dynamic equilibrium and that neither kinetics nor mass transport limits SCN^- equilibration with the solvent. The blue curve at the bottom of Figure 3A shows that washing the ZnSe-SCN NCs with an excess of ^{15}N isotopically labeled potassium thiocyanate ($KSC^{15}N$) in acetone leads to a shift in the IR frequency of both the CN stretching peaks. The shift is precisely that expected from the increase in the oscillator's reduced mass, indicating quantitative exchange of the original SCN^- for $SC^{15}N^-$. The red curve in this panel demonstrates that washing the sample with acetone does not significantly change the ratio of free and bound peaks or the integrated intensity of the CN stretch.

Published values for the molar absorptivity of CdSe NCs[52] make it possible to quantify the number of SCN^- anions observed per NC by IR spectroscopy. In the blue curve in Figure 3B, the IR spectrum is shown for a sample of exchanged CdSe NCs in DMSO, where the absorbance of the first excitonic peak in the visible is measured for the sample and used to scale the IR data to an NC concentration of 1 mM. In contrast to the example with ZnSe, there is no distinct peak observed in the IR that can be assigned to the ionically bound form of the

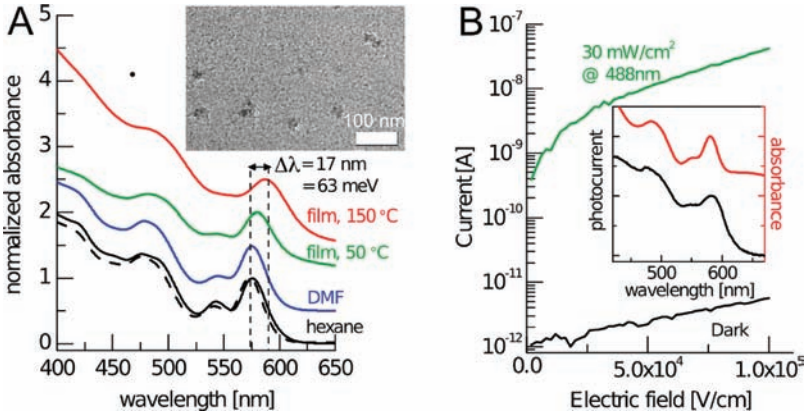

Figure 4. UV−vis absorption spectra and photocurrent measurements of CdSe NCs. (A) CdSe NCs with the original long-chain ligands dispersed in hexanes (solid black) or NH_4SCN-treated and dispersed in DMF (blue). After dispersion in DMF, NCs were back-exchanged with organic ligands and redispersed in hexanes (dashed black). Alternatively, DMF-dispersed CdSe-SCN was evaporated at 50 °C to form a thin film on a glass substrate (green) or further annealed for 20 min at 150 °C (red). Inset: SEM image of a CdSe-SCN film made identically to the sample depicted in green. (B) Photoconductivity of a CdSe-SCN thin film on a quartz substrate with 150 μm wide Au electrodes separated by 10 μm. Dark current (black) and photocurrent for 488 nm illumination at 30 mW/cm^2 (green). Inset: spectral response and absorption spectra measured for the same sample.

thiocyanate, with the possible exception of the low, broad shoulder at the base of the main peak. Nevertheless, a consistent minimum number of SCN^- anions are observed to balance the charge sites on the NC surface. The dashed black curve depicts the spectrum of NH_4SCN at a known concentration in DMSO, which is used to establish the oscillator strength of free SCN^- anions. A comparison of the relative integrated area of the blue curve, which is assigned to free SCN^- anions that are charge-balanced by the NC, and the dashed black curve yields an equivalent concentration of SCN^- of slightly greater than 30 mM for the NC sample, i.e., >30 SCN^- anions per NC. The red curve demonstrates that additional washing of the NCs with acetone does not significantly reduce the integrated area. The same limiting value after washing is also observed if the initial molar ratio of NH_4SCN used in the exchange step is doubled.

To explain these observations, we propose that SCN^- is either bound to or electrostatically balanced by positive charge sites on the NC surface due to stoichiometric imbalances characterized by the formula $(CdSe)_nCd_m$, with m such sites available. It should be noted that our data could also be rationalized assuming a stoichiometrically balanced NC with topologically isolated, undercoordinated Cd sites bearing positive charge and an equal number of isolated, undercoordinated selenium sites bearing negative charge. However, the model based on stoichiometric imbalance is supported by previous observations in CdSe NCs that demonstrated Cd:Se ratios of 1.1 to 1.2 in favor of Cd by Rutherford backscattering[58] and wavelength-dispersive X-ray spectroscopy, respectively.[59] The value obtained by IR of >30 SCN^- binding sites per NC for a 3.9 nm diameter NC sample compares favorably with an NMR study of aqueous-synthesized 3.5 nm CdSe NCs that found 23 binding sites per NC for anionic butanethiolate ligands.[60] A role for positively charged Cd sites is also consistent with more recent NMR reports that show that the conjugate bases of different acidic surfactants are present in the byproducts of ligand displacement reactions on colloidal NCs.[61,62] A model for the mechanism of colloidal stabilization emerges from the combination of the ζ potential and the solution- and solid-state IR measurements. Positively charged metal sites on the NC surface bind the anionic SCN^- counterion in the solid state, as indicated by the dependence of the CN stretching frequency on the identity of the metal (Figure 2). When highly polar solvents are added to CdSe-SCN or ZnSe-SCN, the large Debye length in these solvents enables the dissociation of SCN^- anions from the surface of the NCs (Figure 3). In support of this we note that cadmium−thiocyanate bonds are labile in DMSO (see refs 57 and 63 and the Supporting Information, Figures S5 and S6). The localized positive charges on the NC surface and their nonspecifically associated SCN^- counterions comprise an electrostatic double layer manifested in the positively charged ζ potential (Figure 1) and are ultimately responsible for the electrostatic repulsion between NCs.

Enhanced Interparticle Coupling in Thin Films: Solution Exchange. In addition to its utility as a spectroscopic probe, the short interparticle separation provided by SCN (Supporting Information, Figure S2) is beneficial for device applications of semiconductor and metal NC ensembles. NC films drop-cast from a dispersion of Au NCs with long-chain organic ligands are highly insulating, with typical values for the conductivity in the range of 10^{-9} Ω^{-1} cm^{-1}.[11,33] Drop-casting SCN-capped Au NCs from DMSO at 60 °C under reduced pressure, however, makes highly conductive films that, measured with a multimeter, give conductivities of $(2 \pm 0.7) \times 10^3$ Ω^{-1} cm^{-1}, an increase by a factor of >10^{12} from that of the long-chain ligands. While still 100-fold lower than the conductivity of bulk Au,[64] the conductivity is 10-fold higher than previously reported for films made from metal chalcogenide-capped Au NCs spin-cast at room temperature.[33] The higher processing temperature for the SCN-capped Au NC films may be partially responsible for this difference; however, we note that wide-angle X-ray measurements of identically prepared films indicate the NC size is not changed under these conditions (Supporting Information, Figure S2).

For CdSe NCs, ligand exchange preserves the ensemble monodispersity and solution dispersibility while giving rise to substantially improved interparticle coupling in NC thin films. In Figure 4A, the spectrum after ligand exchange and redispersion in DMF under nitrogen (blue curve) is compared to the original absorption spectrum (solid, black curve). The well-resolved electronic absorption spectrum characteristic of highly monodisperse CdSe is observed in both spectra. The exchange process is reversible: a spectrum of the SCN-capped CdSe NCs,

redispersed into hexanes by adding excess oleic acid and octadecylamine (dashed, black curve), shows that the features remain nearly unchanged. SEM images of thin films of CdSe-SCN evaporated from dispersions in DMF (inset of Figure 4A) show dense packing of individual NCs over wide areas. An increase in electronic coupling in films cast from DMF or DMSO is evident spectroscopically. Transmission UV−vis absorption spectra of thiocyanate-exchanged CdSe NC films, shown after annealing at 50 or 150 °C (green and red curves, respectively), progressively shift to the red, with the energy of the first exciton peak shifted as far as 63 meV relative to the as-synthesized value in hexanes solution. The change in the spectroscopic energy is worth noting as it indicates an *increase* in the electronic coupling; however, to go from this to a quantitative estimate of the electronic coupling energy between NCs requires a comprehensive model, which we do not develop here. Such a model would have to include, among other considerations, contributions to the bathochromic shifts from changes in the local dielectric environment after original ligand removal and film formation.

NH_4SCN treatment increases the electrical conductivity of thin films of semiconductor NCs to a higher degree than other widely employed small ligand treatments.[26−28] The green curve in Figure 4B represents the photoconductivity of films of CdSe-SCN NCs under 30 mW/cm^2 illumination at 488 nm. From this curve and the dimensions of the channel, a photoconductivity of 10^{-5} Ω^{-1} cm^{-1} is calculated at 100 kV/cm. This photoconductivity is 10^3 times larger than values calculated from recent literature reports of butylamine-treated CdSe NCs under similar measurement conditions.[65] Comparing the black and green curves, the ratio of the current in the illuminated versus dark states, I_{photo}/I_{dark}, is 10^3 at 10 V bias (corresponding to 10 kV/cm), rising to 10^4 at 100 V, making it equal to or better than reported values for butylamine-treated CdSe NCs.[15] The favorable transport and sensitivity characteristics, necessary to make this an efficient photodetector, are possible without a loss of the spectral tunability afforded by quantum confinement: the inset of Figure 4B demonstrates that the spectral response for CdSe-SCN films, taken at 1 V bias, closely traces the optical absorption spectrum taken of the same sample in an area not covered by the electrodes. We note that the resolution of the spectral response data is limited by the instrument band pass.

Table 1. Hall Effect Measurements of 7.5 nm PbTe NC Films

thickness (μm)	resistivity ($\Omega\cdot$cm)	carrier concentration (cm^{-3})	carrier mobility (cm^2/(V·s))	carrier type
1.6 ± 0.2	5.9 ± 0.08	(4.0 ± 1.3) × 10^{17}	2.8 ± 0.7	holes

Enhanced Interparticle Coupling in Thin Films: Solid Exchange. The increased electronic coupling seen in solution-exchanged CdSe NCs is general to both solution and solid thiocyanate exchange of various semiconductor NCs. For example, NH_4SCN treatment of 6.2 nm CdTe NC solids causes a shift in the first absorption maximum from as-deposited tetradecylphosphonic acid-capped films of 20 meV, which is further increased to 53 meV by annealing at 100 °C (Supporting Information, Figure S7). For PbTe NCs deposited into films with the original ligands, the resistivity has been reported as 10^{13} $\Omega\cdot$cm.[47] A >10^{13} decrease in resistivity with NH_4SCN treatment demonstrates the dramatic enhancement of interparticle coupling after ligand exchange, enabling the first measurement to our knowledge of the Hall effect in nonsintered NC thin films (Table 1). In our hands, treatment of PbTe with other small ligands such as hydrazine does not sufficiently increase the carrier mobility to generate a measurable Hall voltage. NH_4SCN treatment, on the other hand, results in high Hall effect mobility, μ_{Hall}, of 2.8 ± 0.7 cm^2/(V·s) in 7.5 nm PbTe NC films.

High-Performance Thin-Film NC Transistors. We demonstrate the utility of the solution-exchanged, thiocyanate-capped CdSe NCs by spin-coating NC dispersions from DMF to fabricate the semiconducting channels of thin-film FETs. In Figure 5A, the top-contact, bottom-gate configuration of the device is shown schematically, along with an SEM image of the channel, showing that spin-coating forms uniform thin films across micrometer-scale channel dimensions. Annealing of the devices under nitrogen leads to changes in the surface chemistry indicated by a decrease in the integrated area of the thiocyanate stretch, shown in the Supporting Information, Figure S8A, and increased electron mobility, plotted in Figure S8B, which by 250 °C is quite favorable for device applications. The decomposition or desorption of the thiocyanate group observed at this temperature would be expected to allow for decreased interparticle distance and hence increased electronic coupling, which may explain part of the increase in mobility. While partial sintering or particle "necking" is conceivable at these temperatures, characteristics of individual particles are observed in two separate experiments. In the inset of Figure 5C, the UV−vis transmission spectrum of an identically prepared film on a sapphire substrate demonstrates that annealing at 250 °C for 10 min preserves the excitonic features indicative of NC quantum

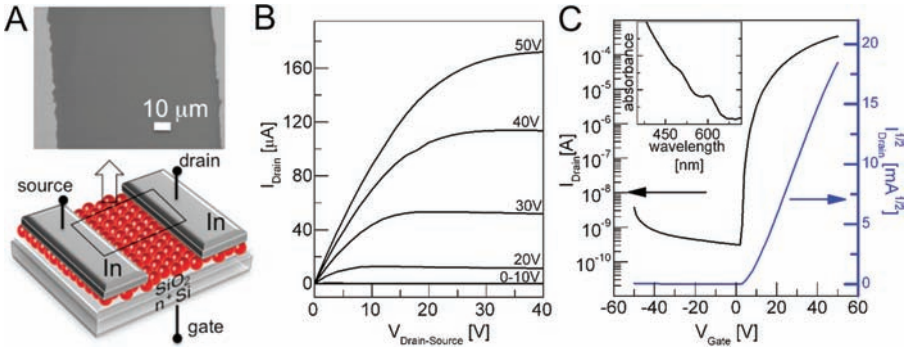

Figure 5. CdSe-SCN field-effect transistor characterization for a device annealed at 250 °C. (A) Schematic of the transistor geometry, showing from bottom to top the doped Si substrate, SiO_2 thermal oxide, spin-cast CdSe-SCN layer, and indium top source and drain electrodes. SEM image of the channel, showing edges of indium electrodes on either side. (B) Typical drain−source current as a function of V_D at different values of V_G. (C) I_D as a function of V_G at a drain−source bias of 50 V. The left *y*-axis is on the log scale, and the right *y*-axis is on the square root scale. Inset: UV−vis absorption spectrum of an identically processed sample on sapphire.

dx.doi.org/10.1021/ja206303g |*J. Am. Chem. Soc.* 2011, 133, 15753–15761

confinement, and an SEM image of such a film in the Supporting Information, Figure S9, is also suggestive of preserved NC individuality.

Figure 5B depicts representative drain current (I_D) versus source−drain voltage (V_{DS}) characteristics as a function of the applied gate voltage, indicating CdSe-SCN NC thin films form *n*-channel FETs. The devices operate in accumulation mode upon application of a positive gate bias as the concentration of majority carrier electrons contributing to I_D increases. The devices show well-behaved FET characteristics, rising linearly at low V_{DS} and saturating at high V_{DS} as the channel is pinched off near the drain electrode. Device operation is adequately modeled by standard FET equations,[66] which are employed with the I_D and $I_D^{1/2}$ vs V_G data in Figure 5C to calculate the field-effect mobility for electrons (μ_e), current modulation (I_{ON}/I_{OFF}), threshold voltage (V_T), and subthreshold swing (S). The devices show an average μ_e of 1.5 ± 0.7 $cm^2/(V\cdot s)$, with the best mobilities to date of 3 $cm^2/(V\cdot s)$ measured across 31 independent devices. For a typical device, such as that shown in Figure 5, the mobilities calculated in the linear and saturation regimes, μ_{lin} and μ_{sat}, are within 10% of each other. I_{on}/I_{off} is $\sim 10^6$, with a threshold voltage of 7 V. The subthreshold swing, a critical metric for how well the device turns on and off, is 0.73 V/decade, comparable to the industry standard for amorphous Si-based thin-film FETs.[67]

CONCLUSION

We demonstrate thiocyanate as a capping group for a broad range of NC materials, capable of stabilizing NC colloids in polar solvents. Infrared spectroscopy of the thiocyanate ligand furnishes an incisive reporter of the chemical nature of the NC surface, providing a direct measure of the number of ligand binding sites and their atom type and charge. In future work we seek to leverage this probe of NC chemistry and electronics to optimize NC materials and their interfaces for device applications.

Thiocyanate is a compact ligand, providing short interparticle separation and increased interparticle coupling in NC thin films, as evidenced by large bathochromic shifts in NC absorption and dramatically increased film conductivities and carrier mobilities. Ammonium thiocyanate treatment of NCs promises an attractive, environmentally benign route for thin-film electronics, compatible with large-scale use. Employing thiocyanate-capped CdSe NCs, we realize high-performance NC thin-film photodetectors and field-effect transistors. We are currently optimizing the performance of thiocyanate NC thin films for solar cell, photodetector, thermoelectric, and transistor applications.

ASSOCIATED CONTENT

Supporting Information. Additional experimental information and figures. This material is available free of charge via the Internet at http://pubs.acs.org

AUTHOR INFORMATION

Corresponding Author
kagan@seas.upenn.edu

ACKNOWLEDGMENT

We thank E. Ashley Gaulding for assistance with Hall effect measurements and Adriel Koschitzky, Taejong Paik, Tom Gordon, Yijin Kang, Jun Chen, and Bianca Datta for assistance with materials testing. Photos were taken by Felice Macera. A.T.F., W.-k.K., B.T.D., M.R.C., C.B.M., and C.R.K. are grateful for support from the NSF Solar Program under Award No. DMS-0935165. D.K.K. acknowledges support from NSF-CBET (Grant CBET-0854226), and D.-K.K. recognizes support from NSF MRSEC (Grant DMR-0520020). S.J.O. and D.C.R. acknowledge support from the U.S. Department of Energy Office of Basic Energy Sciences, Division of Materials Science and Engineering, under Award No. DE-SC0002158. D.C.R. acknowledges additional support from the NSF-IGERT program (Grant DGE-0221664). X.Y. recognizes support from the Office of Naval Research MURI program under Award No. ONR-N00014-10-1-0942, and V.D.-N. acknowledges support from the Department of Energy, DOE Office of ARPA-E, Award No. DE-AR0000123. The microscope facilities used in this work are supported in part by NSF MRSEC under Award No. DMR-0520020.

REFERENCES

(1) Murray, C. B.; Norris, D. J.; Bawendi, M. G. *J. Am. Chem. Soc.* **1993**, *115*, 8706–8715.
(2) Yu, W. W.; Wang, Y. A.; Peng, X. *Chem. Mater.* **2003**, *15*, 4300–4308.
(3) Manna, L.; Milliron, D. J.; Meisel, A.; Scher, E. C.; Alivisatos, A. P. *Nat. Mater.* **2003**, *2*, 382–385.
(4) Park, Y. I.; Piao, Y.; Lee, N.; Yoo, B.; Kim, B. H.; Choi, S. H.; Hyeon, T. *J. Mater. Chem.* **2011**, *21*, 11472–11477.
(5) Murray, C. B.; Kagan, C. R.; Bawendi, M. G. *Annu. Rev. Mater. Sci.* **2000**, *30*, 545–610.
(6) Carbone, L.; Nobile, C.; De Giorgi, M.; Sala, F. D.; Morello, G.; Pompa, P.; Hytch, M.; Snoeck, E.; Fiore, A.; Franchini, I. R.; Nadasan, M.; Silvestre, A. F.; Chiodo, L.; Kudera, S.; Cingolani, R.; Krahne, R.; Manna, L. *Nano Lett.* **2007**, *7*, 2942–2950.
(7) Shevchenko, E.; Talapin, D.; Murray, C.; O'brien, S. *J. Am. Chem. Soc.* **2006**, *128*, 3620–3637.
(8) Baker, J. L.; Widmer-Cooper, A.; Toney, M. F.; Geissler, P. L.; Alivisatos, A. P. *Nano Lett.* **2010**, *10*, 195–201.
(9) Urban, J.; Talapin, D.; Shevchenko, E.; Kagan, C.; Murray, C. *Nat. Mater.* **2007**, *6*, 115–121.
(10) Murray, C. B.; Kagan, C. R.; Bawendi, M. G. *Science* **1995**, *270*, 1335–1338.
(11) Zabet-Khosousi, A.; Dhirani, A.-A. *Chem. Rev.* **2008**, *108*, 4072–4124.
(12) Gur, I.; Fromer, N.; Geier, M.; Alivisatos, A. *Science* **2005**, *310*, 462–465.
(13) Luther, J. M.; Law, M.; Beard, M. C.; Song, Q.; Reese, M. O.; Ellingson, R. J.; Nozik, A. J. *Nano Lett.* **2008**, *8*, 3488–3492.
(14) McDonald, S. A.; Konstantatos, G.; Zhang, S.; Cyr, P. W.; Klem, E. J. D.; Levina, L.; Sargent, E. H. *Nat. Mater.* **2005**, *4*, 138–142.
(15) Oertel, D. C.; Bawendi, M. G.; Arango, A. C.; Bulović, V. *Appl. Phys. Lett.* **2005**, *87*, 213505.
(16) Colvin, V. L.; Schlamp, M. C.; Alivisatos, A. P. *Nature* **1994**, *370*, 354–357.
(17) Coe, S.; Woo, W.-K.; Bawendi, M.; Bulović, V. *Nature* **2002**, *420*, 800.
(18) Klein, D. L.; Roth, R.; Lim, A. K. L.; Alivisatos, A. P.; McEuen, P. L. *Nature* **1997**, *389*, 699–701.
(19) Talapin, D. V.; Murray, C. B. *Science* **2005**, *310*, 86–89.
(20) Yu, D.; Wang, C.; Guyot-Sionnest, P. *Science* **2003**, *300*, 1277–1280.
(21) Yu, D.; Wehrenberg, B. L.; Jha, P.; Ma, J.; Guyot-Sionnest, P. *J. Appl. Phys.* **2006**, *99*, 104315.
(22) Martin, J.; Nolas, G. S.; Zhang, W.; Chen, L. *Appl. Phys. Lett.* **2007**, *90*, 222112.
(23) Wang, R. Y.; Feser, J. P.; Lee, J.-S.; Talapin, D. V.; Segalman, R.; Majumdar, A. *Nano Lett.* **2008**, *8*, 2283–2288.

(24) Ko, D.-K.; Kang, Y.; Murray, C. B. *Nano Lett.* **2011**, *11*, 2841–2844.
(25) Sun, S.; Murray, C. B.; Weller, D.; Folks, L.; Moser, A. *Science* **2000**, *287*, 1989–1992.
(26) Andres, R. P.; Bielefeld, J. D.; Henderson, J. I.; Janes, D. B.; Kolagunta, V. R.; Kubiak, C. P.; Mahoney, W. J.; Osifchin, R. G. *Science* **1996**, *273*, 1690–1693.
(27) Jarosz, M. V.; Porter, V. J.; Fisher, B. R.; Kastner, M. A.; Bawendi, M. G. *Phys. Rev. B* **2004**, *70*, 195327.
(28) Law, M.; Luther, J. M.; Song, Q.; Hughes, B. K.; Perkins, C. L.; Nozik, A. J. *J. Am. Chem. Soc.* **2008**, *130*, 5974–5985.
(29) Kalyuzhny, G.; Murray, R. W. *J. Phys. Chem. B* **2005**, *109*, 7012–7021.
(30) Soreni-Harari, M.; Mocatta, D.; Zimin, M.; Gannot, Y.; Banin, U.; Tessler, N. *Adv. Funct. Mater.* **2010**, *20*, 1005–1010.
(31) Leatherdale, C. A.; Kagan, C. R.; Morgan, N. Y.; Empedocles, S. A.; Kastner, M. A.; Bawendi, M. G. *Phys. Rev. B* **2000**, *62*, 2669.
(32) Lee, J.-S.; Kovalenko, M. V.; Huang, J.; Chung, D. S.; Talapin, D. V. *Nat. Nanotechnol.* **2011**, *6*, 348–352.
(33) Kovalenko, M. V.; Scheele, M.; Talapin, D. V. *Science* **2009**, *324*, 1417–1420.
(34) Dong, A.; Ye, X.; Chen, J.; Kang, Y.; Gordon, T.; Kikkawa, J. M.; Murray, C. B. *J. Am. Chem. Soc.* **2011**, *133*, 998–1006.
(35) Nag, A.; Kovalenko, M. V.; Lee, J.-S.; Liu, W.; Spokoyny, B.; Talapin, D. V. *J. Am. Chem. Soc.* **2011**, *133*, 10612–10620.
(36) Bailey, R. A.; Kozak, S. L.; Michelsen, T. W.; Mills, W. N. *Coord. Chem. Rev.* **1971**, *6*, 407–445.
(37) Hu, J.-W.; Li, J.-F.; Ren, B.; Wu, D.-Y.; Sun, S.-G.; Tian, Z.-Q. *J. Phys. Chem. C* **2007**, *111*, 1105–1112.
(38) Yao, J.-L.; Xu, X.; Wu, D.-Y.; Xie, Y.; Ren, B.; Tian, Z.-Q.; Pan, G.-P.; Sun, D.-M.; Xue, K.-H. *Chem. Commun.* **2000**, 1627–1628.
(39) Voitekhovich, S. V.; Talapin, D. V.; Klinke, C.; Kornowski, A.; Weller, H. *Chem. Mater.* **2008**, *20*, 4545–4547.
(40) Yu, W. W.; Peng, X. *Angew. Chem., Int. Ed.* **2007**, *46*, 2559.
(41) Qu, L. H.; Peng, X. G. *J. Am. Chem. Soc.* **2002**, *124*, 2049–2055.
(42) Lin, S. L.; Pradhan, N.; Wang, Y. J.; Peng, X. G. *Nano Lett.* **2004**, *4*, 2261–2264.
(43) Winnischofer, H.; Rocha, T. C. R.; Nunes, W. C.; Socolovsky, L. M.; Knobel, M.; Zanchet, D. *ACS Nano* **2008**, *2*, 1313–1319.
(44) Chen, Z.; Moore, J.; Radtke, G.; Sirringhaus, H.; O'Brien, S. *J. Am. Chem. Soc.* **2007**, *129*, 15702–15709.
(45) Hines, M. A.; Scholes, G. D. *Adv. Mater.* **2003**, *15*, 1844–1849.
(46) Yu, W. W.; Falkner, J. C.; Shih, B. S.; Colvin, V. L. *Chem. Mater.* **2004**, *16*, 3318–3322.
(47) Urban, J. J.; Talapin, D. V.; Shevchenko, E. V.; Murray, C. B. *J. Am. Chem. Soc.* **2006**, *128*, 3248–3255.
(48) Ye, X.; Chen, J.; Murray, C. B. *J. Am. Chem. Soc.* **2011**, *133*, 2613–2620.
(49) Murray, C. B.; Sun, S. H.; Doyle, H.; Betley, T. *MRS Bull.* **2001**, *26*, 985–991.
(50) Yarema, M.; Kovalenko, M. V.; Hesser, G.; Talapin, D. V.; Heiss, W. *J. Am. Chem. Soc.* **2010**, *132*, 15158–15159.
(51) Pallavicini, P.; Dacarro, G.; Galli, M.; Patrini, M. *J. Colloid Interface Sci.* **2009**, *332*, 432–438.
(52) Yu, W. W.; Qu, L.; Guo, W.; Peng, X. *Chem. Mater.* **2003**, *15*, 2854–2860.
(53) Everett, D. H. *Pure Appl. Chem.* **1972**, *31*, 577–638.
(54) Burmeister, J. *Coord. Chem. Rev.* **1990**, *105*, 77–133.
(55) Baranyi, A. D.; Makhija, R.; Onyszchuk, M. *Can. J. Chem.* **1976**, *54*, 1189–1196.
(56) Emeléus, H. J.; Sharpe, A. G. *Advances in Inorganic Chemistry and Radiochemistry*; Academic Press: New York, 1975.
(57) Kargol, J. A.; Crecely, R. W.; Burmeister, J. L. *Inorg. Chem.* **1979**, *18*, 2532–2535.
(58) Taylor, J.; Kippeny, T.; Rosenthal, S. J. *J. Cluster Sci.* **2001**, *12*, 571–582.
(59) Dabbousi, B. O.; Rodriguez-Viejo, J.; Mikulec, F. V.; Heine, J. R.; Mattoussi, H.; Ober, R.; Jensen, K. F.; Bawendi, M. G. *J. Phys. Chem. B* **1997**, *101*, 9463–9475.
(60) Majetich, S. A.; Carter, A. C.; Belot, J.; McCullough, R. D. *J. Phys. Chem.* **1994**, *98*, 13705–13710.
(61) Owen, J. S.; Park, J.; Trudeau, P.-E.; Alivisatos, A. P. *J. Am. Chem. Soc.* **2008**, *130*, 12279–12281.
(62) Kopping, J. T.; Patten, T. E. *J. Am. Chem. Soc.* **2008**, *130*, 5689–5698.
(63) Persson, I.; Iverfeldt, Å.; Ahrland, S.; Persson, I.; Spahiu, K. *Acta Chem. Scand.* **1981**, *35a*, 295–304.
(64) Lide, D. R. *CRC Handbook of Chemistry and Physics*, 90th ed.; CRC Press: Boca Raton, FL, 2009.
(65) Geyer, S.; Porter, V. J.; Halpert, J. E.; Mentzel, T. S.; Kastner, M. A.; Bawendi, M. G. *Phys. Rev. B* **2010**, *82*, 155201.
(66) Sze, S. M. *Semiconductor Devices: Physics and Technology*, 2nd ed.; Wiley: New York, 2001.
(67) Kagan, C. R.; Andry, P. *Thin-Film Transistors*, 1st ed.; CRC Press: Boca Raton, FL, 2003.